The International Journal of Advanced Manufacturing Technology (2018) 96:1859–1873
https://doi.org/10.1007/s00170-018-1681-y

ORIGINAL ARTICLE

Reducing deformation, stress, and tool wear during milling processes using simulation-based multiobjective optimization

J. Montalvo-Urquizo[1] · C. Niebuhr[2] · A. Schmidt[2] · M. G. Villarreal-Marroquín[1]

Received: 30 August 2017 / Accepted: 29 January 2018 / Published online: 15 February 2018

Abstract
This paper presents the optimization of a dry machining process where thermomechanical effects like shape deviations and a time-dependent domain are major challenges. First, the simulation model to compute finite element approximations to a general milling process is presented. The model includes a submodel (dexel model) for material removal and process forces and heat flux introduced by the machining tool. In a second part, we present a multiobjective optimization algorithm based on metamodels that serve as a tool to identify the process parameters that improve processes with different performance measures that exhibit conflicting behavior. With this metamodel-based optimization method, we avoid the use of a large number of high-fidelity computer simulations, which are commonly computationally expensive. The approach is tested on two case studies for optimizing (a) workpiece deformation and equivalent stress after milling, and (b) shape error and tool wear.

Keywords Milling · Multiobjective optimization · Thermomechanics · Adaptive FEM

1 Introduction

For manufacturing businesses to be successful in the global market, they must strive to deliver high-quality products at the lowest possible cost. One approach to select the processing conditions to achieve these goals is to run experiments on the manufacturing floor. Such experimentation is usually costly and requires considerable amount of time and effort, which may not be feasible during production [6]. Alternatively, advanced computer simulations can be used to represent the processes. Such computer simulations along side with optimization methods are used to identify the values of the controllable processing variables that optimize the relevant performance measures (PMs). In this work, we present an integrated framework to find optimal process parameters for a milling operation using a combination of metaheuristic optimization models and thermomechanical finite element (FEM) simulations.

Milling of metallic components is a machining operation based on the removal of material using a multi-edged rotating tool and a relative motion of the tool and the component that generates the so-called feed of the milling process, [19, 21]. Commonly, the feed and turning velocities of the machining process are operated using a computer numerical control (CNC) system on a NC machining center. The resulting geometry of the milled component is determined by the feed trajectory of the machining process removing a chip of material in each pass of the cutting insert, [3–5]. The left draw on Fig. 1 illustrates a milling rotating tool and its main parameters.

It is well-known that the cutting of material chips and the friction of the cutting tool with the workpiece produces heat. The right side of Fig. 1 illustrates the thermomechanical deformation effect of a milled part. In some cases, the reached temperatures may lead to non-controlled material deformation and results in undesired shape deviations of the

✉ J. Montalvo-Urquizo
jonathan.montalvo@cimat.mx

A. Schmidt
schmidt@math.uni-bremen.de

M. G. Villarreal-Marroquín
maria.villarreal@cimat.mx

[1] CIMAT-Monterrey, CONACYT and Centro de Investigación en Matemáticas, Alianza Centro 502, Parque de Investigación e Innovación Tecnológica, 66629 Monterrey, Mexico

[2] Center for Industrial Mathematics and MAPEX Center for Materials and Processes, University of Bremen, Bibliothekstraße 1 (MZH), 28359 Bremen, Germany

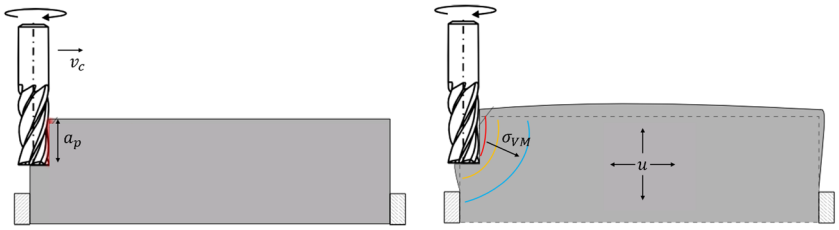

Fig. 1 Left: milling rotating tool and its main parameters illustrated over the original geometry of the component. Right: illustration of thermomechanical effects on the component resulting in thermal expansion and stress

machined product. Hence, there is big interest on generating simulation tools to better understand the thermal effects arising during the milling process, as well as to identify the process parameters that minimize such effects.

In this sense, a thermomechanical simulation in which the temperature generated is used as input to simulate the thermal expansion and the corresponding mechanical deformation of the workpiece is needed [3]. In this work, we consider adaptive FEM simulations implemented in ALBERTA [17] that share the coupled thermomechanical spirit of previous works on heat treatment [20], laser welding [11], and forming [12].

Joining simulation and optimization for defining the best possible process parameters is an actual need in current engineering practice [23, 25, 26]. This often comes together with the issue of evaluating an optimization functional at many candidate solutions which request to run a complete simulation that is computationally expensive [8]. As for many other real processes, a milling simulation can require a large amount of computation and, in dependence of the process complexity, a single simulation evaluation can take minutes to even days.

For these type of problems, optimization methodologies are typically based on surrogate models (or metamodels) which are mathematical models that try to mimic the behavior of the simulation model based on a limited number of observations [1, 10, 25]. Metamodels help reduce the computational effort required to evaluate the performance measures at different process conditions, as they are faster to evaluate than the simulation model. Surrogate models are also convenient for cases when it is only possible to use experimental data and a single process evaluation is expensive and time-consuming. Therefore, by utilizing surrogate models, it is possible to use an optimization technique that requires the evaluation of the process at a high number of processing conditions.

Among the most commonly used surrogate models, we can find are response surface, kriging, radial basis functions (RBF), and artificial neural networks. Reviews of surrogate models used in optimization via simulation can be found in [1, 10, 18, 25].

Li et. al [9] constructed empirical models to estimate the relationship between tool life, residual stress, and surface roughness with different milling parameters for titanium alloys. Later, the empirical models were used to optimize multiple performance measures using genetic algorithms (GA). Qu et al. [14] used experimental data to construct regression models to estimate cutting force and surface roughness of thin-wall machined plates. Then, they used the statistical models with a multiobjective GA to identify the machining parameters that optimize the performance measures. An extensive literature review of different models and optimization methods that have been used to improve milling processes is presented in [15].

In the following sections, the milling process and its thermomechanical simulation (Section 2), the metamodel-based optimization method (Section 3), and two case studies where simulation and optimization are merged to obtain the set of optimal PMs (Section 4) are presented. Finally, we present some conclusive remarks and future work in Section 5.

2 Numerical process simulation

In this work, we use an adaptive FEM simulation for the milling process considering the combination of a dexel model and the thermal and mechanical equations as presented in [3]. The models consist of an extension of a classical NC-simulation to emulate thermomechanical effects, and it is subdivided into a model for the workpiece and a process model (see Fig. 2).

The workpiece model describes the current state of the workpiece in geometrical and thermomechanical aspects (Fig. 2 left). A material removal simulation via a dexel model allows to efficiently represent the change of the geometrical representation during the process. A FE-model calculates temperature and linear deformation to represent the thermomechanical workpiece behavior.

The process model has several calculation steps (Fig. 2, right). The cutting conditions are calculated from the geometrical intersection of the tool and the workpiece. With this data, the cutting force and heat flux are predicted and the mechanical and thermal loads are calculated. This changes the boundary shape and the thermal conditions of the FE-model. The shape deviations generated by the material

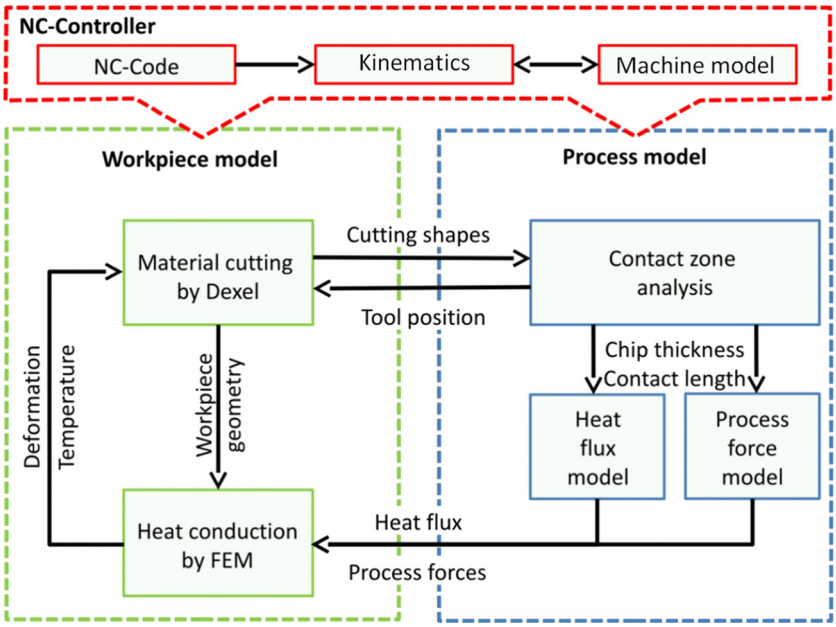

Fig. 2 Detailed information flow of simulation system

cutting process are predicted based on the calculated temperature and deformation behavior of the workpiece. For detailed descriptions of these calculations, see [3–5, 13].

Next, we present the simulated milling process and some FEM simulation results that serve to determine a reduced geometry. The results on the reduced geometry are later used to estimate the performance measures of the workpiece, as will be explained in the optimization part, cf. Section 3.

2.1 Reference process

The machining of a thin-walled part made of 1.1191 steel has been chosen as reference process, and it was already used in different research activities (shown in [4, 5, 13]). The blank part is a rectangular workpiece with 40 mm width, 40 mm depth, 195 mm length, and the percentage of machined material is about 60% (see Fig. 3). The workpiece is clamped at two sides, with one degree of freedom for

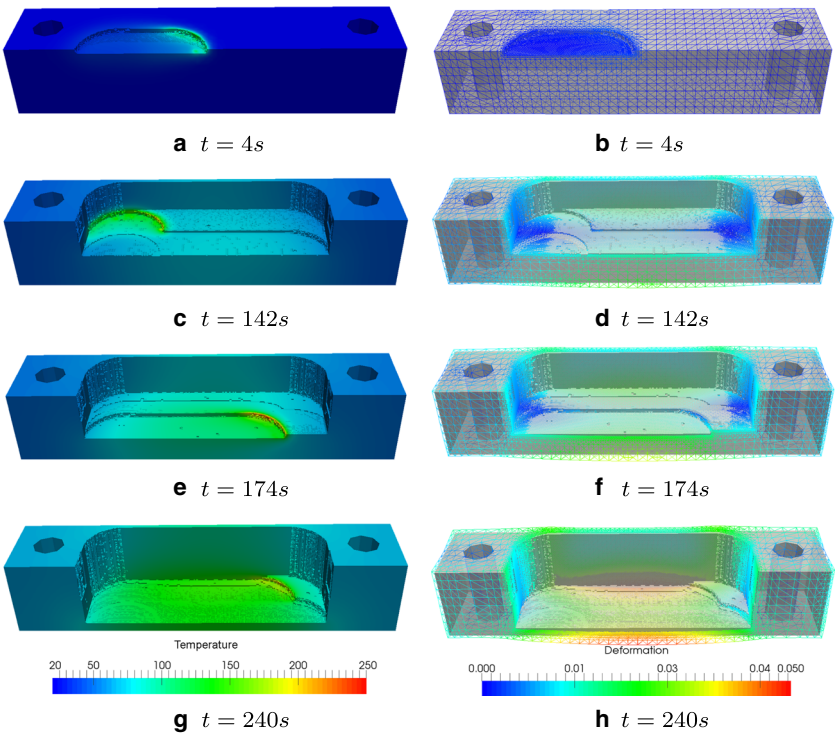

Fig. 3 Simulation of milling (roughing) at different process times. Left: temperature, [°C]. Right: deformation, (mm), using a scaling factor of 100

torsion and translation. The component sides are fixed on a dynamometer in order to measure the clamping effective forces at every moment of the process.

The milling process is divided in two main parts, a roughing and a finishing part. Roughing is the removal of large portions of material out of the workpiece, while the finishing step is a detailed material removal performed at the end with only a small cutting width. The machining strategy is z-level constant, the roughing process is divided in different steps for every level, and a finishing step of the thin wall is performed in one cut and with different number of levels [5].

2.2 Simulation results

The mathematical model implemented for the simulation of the thermomechanical behavior of the workpiece during the machining process has been presented in [13]. This model includes the description of the heat equation and the quasi-stationary linear elasticity equation on a time-dependent domain (due to material removal) with boundaries changing in every time step.

The coupling between the thermal and the mechanical parts of the system of equations is the thermal expansion obtained due to the rising temperature values in regions close to the time-dependent cutting area. This coupled system is implemented using the adaptive finite element toolbox ALBERTA [17].

Figures 3 and 4 show the simulation results for temperature and mechanical deformation at some specific times. The roughing stage is shown in Fig. 3 and the finishing in Fig. 4a–b. Additionally, Fig. 4c–d show the simulated workpiece at the end of the process.

The simulation results have shown to be in accordance with experimental data for both temperature and deformation [5]. The thermomechanical implementation has also been used to simulate more detailed milling processes with thin-walled workpieces for lightweight structures.

For the process optimization, we will use a derived, but further simplified model (see Section 4.1).

3 Multiobjective optimization method

Real manufacturing problems often involve different PMs that exhibit conflicting behavior. For example, the processing conditions that provide the best quality product may not correspond to the lowest production cost. Such situations are strongly present in the milling process that was presented in Section 2. For this reason, we are interested in a methodology to get improvements of a generalized form of performance where several criteria can be studied together.

When multiple conflicting PMs are involved, optimizing a single objective can result in solutions that perform poorly for other objectives. Thus, it is not the best approach to obtain a single solution but rather the set of solutions corresponding to the best compromises. For this, we use the following definition of Pareto solutions:

Definition 1 For the optimization problem of minimizing $(f_1(\mathbf{x}), f_2(\mathbf{x}), \ldots, f_m(\mathbf{x}))$, a feasible solution $\mathbf{x}_1$ is said to dominate $\mathbf{x}_2$ if: $f_i(\mathbf{x}_1) \leq f_i(\mathbf{x}_2)$ $for\, i = 1, \ldots, m$, and $f_i(\mathbf{x}_1) < f_i(\mathbf{x}_2)$ for some $i \in \{1, \ldots, m\}$. The non-dominated solutions are known as *Pareto solutions*. The set of Pareto solutions is known as *Pareto set* (P_{set}) and the corresponding output values form the so-called *Pareto front* (P_{front}).

Given a problem with conflicting PMs, we can focus our attention on finding the Pareto set, and then a decision-maker on a particular moment of the process can select the best solution. This allows for the decision-maker to give different importance to the PMs at any time, once the set of non-dominated solutions is known.

In this work, we use an adapted version of the metamodel-based multiobjective simulation optimization

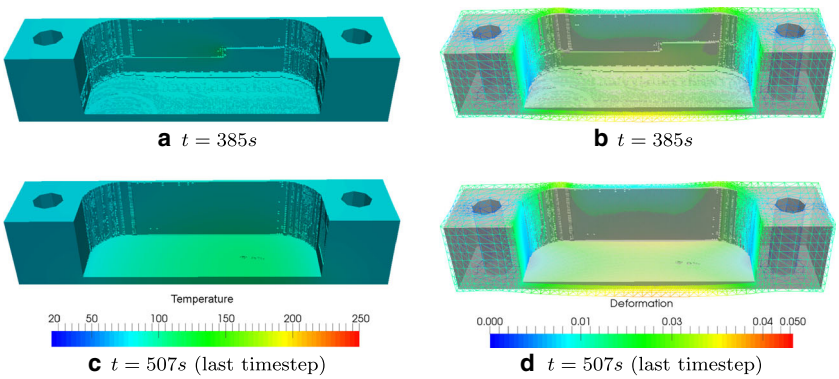

Fig. 4 Simulation of milling during finishing and at the process' end. Left: temperature, [°C]. Right: deformation, (mm), using a scaling factor of 100

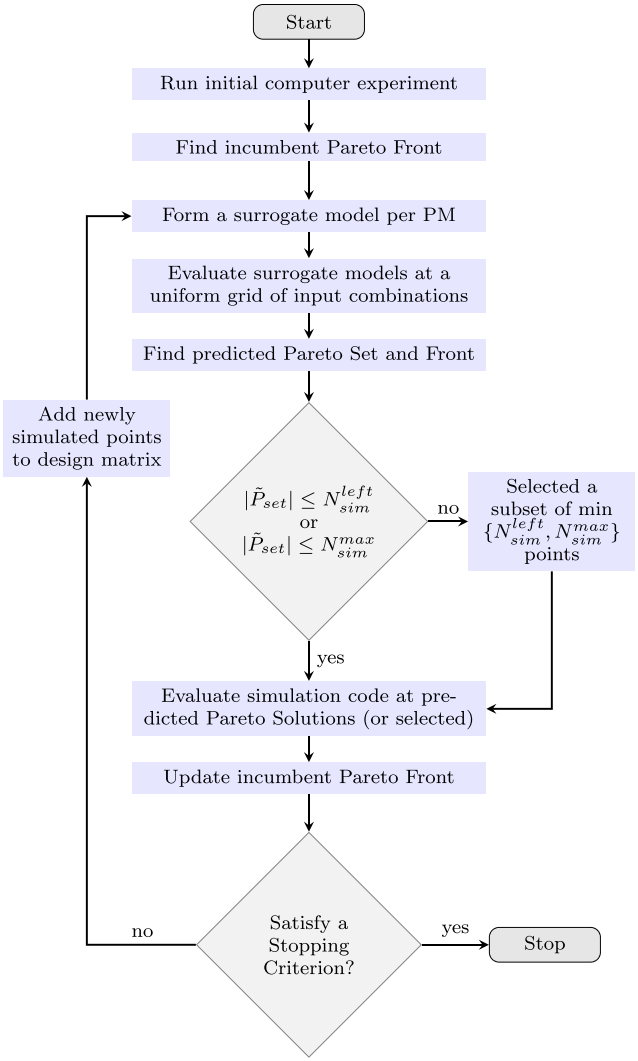

Fig. 5 Multiobjective optimization method flow diagram

method introduced in [22] to optimize two case studies for a milling process.

The method is schematically shown in Fig. 5 and starts by performing an experimental design to collect a set of initial data points, and a simulation run is performed at each point. Then, the set of best compromises between all performance measures is found using definition 1, and it is called *incumbent Pareto front*. Using this, the main iteration steps are the following:

1. Use all available simulated data to fit a metamodel for each PM.
2. Use the metamodels to estimate the value of the PMs for a large uniform set of input combinations.
3. Identify the best compromises between all PMs. Call the corresponding Pareto front, *predicted Pareto front*. The corresponding controllable variables settings are the *predicted Pareto set* ($\tilde{P}_{\text{set}}$).
4. Evaluate the simulation code at predicted Pareto set.
5. Update the incumbent Pareto front (based only on simulated data) using the newly simulated runs and the previous incumbent Pareto front.
6. Evaluate stopping criteria.

It is important to mention that at step 4, if the number of solutions on the predicted Pareto set results to be larger than the remaining number of total simulation runs allowed ($N_{\text{sim}}^{\text{left}}$), or it is larger than the maximum number of simulations allowed per iteration ($N_{\text{sim}}^{\text{max}}$), a subset of $\min\{N_{\text{sim}}^{\text{left}}, N_{\text{sim}}^{\text{max}}\}$ solutions is selected based on a maximin distance criterion using the predicted Pareto front.

At each iteration, a series of stopping criteria are evaluated and if at least one is met, the method stops and reports the incumbent Pareto solutions, otherwise, the newly simulated points are added to the existing simulated set of points and a new iteration begins. The stopping criteria we used in this implementation are as follows:

- Stop if the total number of simulation ($N_{\text{sim}}^{\text{total}}$) allowed is reached
- Stop if the coefficient of determination R^2 of all models is larger than $1 - \varepsilon$
- Stop if no new Pareto solutions are found

Using these iterative steps, at each iteration each metamodel is updated utilizing all available simulated data and are used to approximate a new Pareto set. The updated models are able to predict good approximations of the output responses near the Pareto front.

In [22], it has been shown that this multiobjective optimization method is able to approximate a set of Pareto solutions without having to evaluate a large number of simulations. $15q$ has been shown to be a good upper limit for the total number of simulations ($N_{\text{sim}}^{\text{total}}$), where $q = \max\{m, n\}$, m number of PMs and n number of controllable process variables. For the second stopping criterion we used a value of $\epsilon = 0.01$.

Jin et al. [7] compared several sequential sampling techniques for metamodeling based single objective optimization. They suggest to use a total number of runs of at least $12n$ (if $n < 6$) or $9n$ (if $n \geq 6$). In this work, we used a larger value, $15q$, since the method is intended for multiobjective optimization and the same sampled points are used to fit several independent models (one per PM). In [7], it is also recommended to sample $4n$ (if $n < 6$) or $3n$ if $n \geq 6$ points, at each iteration. Here, the number of points that are sample at each iteration correspond to the number of solutions on the predicted Pareto front (step 3 of main iteration).

However, since this number is commonly large, we usually restrict it to a value of $5q$ when $q < 4$ and $3q$ if $q \geq 4$. This value corresponds to $N_{\text{sim}}^{\max}$.

In [24], this method was used to solve two different cases of an injection molding process. The results were compared with an approach based on Gaussian process metamodels, and it was shown that both methods perform comparably.

4 Case studies for the optimization of milling process

In machining operations, the produced heat results in thermomechanical distortion of the workpiece and thereby in incorrect material removal by the cutting tool. Especially, in machining thin-walled parts for lightweight structures, an additional finishing step is needed as post-process if the resulting shape deviations are larger than a tolerance. In this context, in many cases, the aim for mathematical optimization of a milling process is to minimize the resulting distortion in the produced workpiece, [16]. In addition, tool wearing has a negative effect on surface quality and will also bring additional costs and time for the replacing or reconditioning of the cutting tool. Therefore, minimizing tool wear is also important from the economic standpoint and is why we consider it as one of our process' PMs.

In this Section, we present two optimization case studies of a milling process, each of them with two process' PMs simultaneously.

4.1 Simulation setting for optimization

In order to maintain affordable computational costs for the numerical simulation, we reduced the analyzed workpiece from Section 2.1 to a subdomain of the complete geometry defined as a slice located in the longitudinal center of the workpiece with length 5 mm, as illustrated in Fig. 6. The slice starts being a full block of size $50 \times 50 \times 5$ mm^3 and ends as an L-shaped geometry after the milling process is performed, with a bottom height of 5 mm and side width of 3 mm. Within this small domain, we want to find the optimal process parameters to obtain the smallest deformation, stress, and tool wear.

An important part of the simulation process consists on the generation of an adaptively constructed mesh to represent the time-dependent domain of material. At the beginning of the simulation, the mesh only needs to recreate the blank and consists of only few elements, while during the cutting process, the mesh elements are refined and coarsened in dependence of the location of the cutting line and a posteriori error indicators based on residuals of the heat equation. This strategy has been numerically implemented with a time-dependent discrete domain which is based on the treatment of elements to be declared as inactive when they represent material which has already been removed during the milling.

All processes start using the same mesh with 242 degrees of freedom (DOFs), 600 active tetrahedral elements inside the computational domain and zero non-active elements outside the workpiece. During the process, the number of DOFs and elements increase by the adaptive approximation of the geometry in average up to 22000 DOFs, with 95800 non-active elements outside, and 17800 active elements inside the final workpiece.

The use of different milling parameters generate different computational meshes. Additionally, the computational costs vary due to the different number of time steps to be computed (for slower or faster cuts). The process simulations are running on a workstation with four CPUs (Intel i7-3770, 3.4 GHz) by using one CPU for the finite element simulation and one CPU for the material removal. The typical runtime for a single simulation varies between 20 min and 2 h.

4.2 Case study 1: deformation and stress

The optimization on this case study has two PMs and two process controllable variables. The considered optimization goals are minimize *deformation* (u) and minimize *equivalent stress* (σ_{vM}). As process controllable

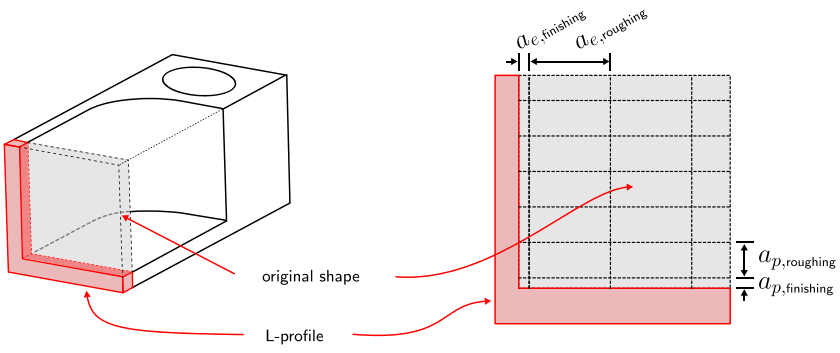

Fig. 6 Model process for optimization, L-shaped domain

Table 1 Fixed process parameter values for case study 1

Variable	Value	
Radial depth of cut	$a_e = 20$	[mm]
Number of teeth	$z = 4$	[-]
Feed rate per tooth	$f_z = 0.20$	[mm/tooth]
Cutter diameter	$D = 40$	[mm]
Average chip thickness	$h_m = 0.20$	[mm]

variables, we considered *cutting velocity* (v_c) and *axial cutting depth* (a_p). The ranges used for the controllable variables correspond to realistic process values and are taken as (100 m/min, 300 m/min] and [5 mm, 30 mm] for v_c and a_p, respectively.

The rest of the process variables are considered as fixed according to the values in Table 1. Other typically considered milling variables like spindle speed, feed speed, and feed per revolution can be calculated using cutting velocity v_c and the values in Table 1.

Deformation, u, is measured as the average of the Euclidean norm at three given points on the outer side of the thin wall near the inner corner of the final workpiece and the stress is measured as the volume averaged von Mises stress σ_{vM} inside a cylinder with radius 1 mm around the inner corner point of the final workpiece.

For the multiobjective optimization algorithm, we used the following parameters: as suggested in [22], the maximum number of evaluations allowed was set to $N_{\text{sim}}^{\text{total}} = 15 \times 2 = 30$, the maximum number of runs per iteration was set as $N_{\text{sim}}^{\max} = 5 \times 2 = 10$, and the lower bound for R^2 was set at 99% ($\varepsilon = 0.01$).

The optimization procedure is as follows:

Initialization

1. *Run initial experimental design*
   The first step of the method is to design and run an experiment to get an initial sample of data points: as suggested in [24], a central composite design is used. The values of the controllable variables and corresponding PMs are shown on Table 2. Figures 7 and 8 show in black dots (1 to 9) the controllable variables and PMs values, respectively.
2. *Find incumbent Pareto front*
   After all data has been collected, the incumbent Pareto front is identified. The incumbent Pareto solutions, from the initial points, is solution 8 (see Fig. 8).

Main iteration, $k = 1$

1. *Form a surrogate model per performance measure*
   A surrogate model is fitted for each PM using all available experimental data. The fitted models used here are multiple linear regression (MLR) models with one degree of freedom, this is $N - 1$ (N, number of data points used to fit the model) regression coefficients are estimated. The coefficients of determination R^2 of the surrogate models are $R_1^2 = 0.9395$ (stress) and $R_2^2 = 0.9974$ (deformation).
2. *Evaluate surrogate models at a uniform grid of input combinations*
   The surrogate models were evaluated at a uniform grid of 10,251 input combinations. The grid of points was constructed as follows: 201 equally spaced levels for cutting velocity (one at each m/min) and 51 levels for axial depth (one at each half millimeter). These levels were selected to acquire a practical difference between simulations. Figure 9 shows the evaluation of the models, where $\hat{f}_1$ estimates (interpolates) stress and $\hat{f}_2$ deformation. The optimization method is implemented in

Table 2 Case study 1: results of initial experimental design

Run	v_c (m/min)	a_p (mm)	σ_{vM} (MPa)	$\|u\|_2$ (mm)	Proc. time (min)
1	100.00	17.50	477.29	0.07094	4.97
2	129.29	8.66	562.30	0.11016	7.13
3	129.29	26.34	346.23	0.03568	2.75
4	200.00	5.00	300.25	0.10849	6.73
5	200.00	17.50	296.99	0.03339	2.48
6	200.00	30.00	249.59	0.02521	1.80
7	270.71	8.66	353.52	0.04596	3.41
8	270.71	26.34	215.12	0.02280	1.32
9	300.00	17.50	219.31	0.02428	1.66

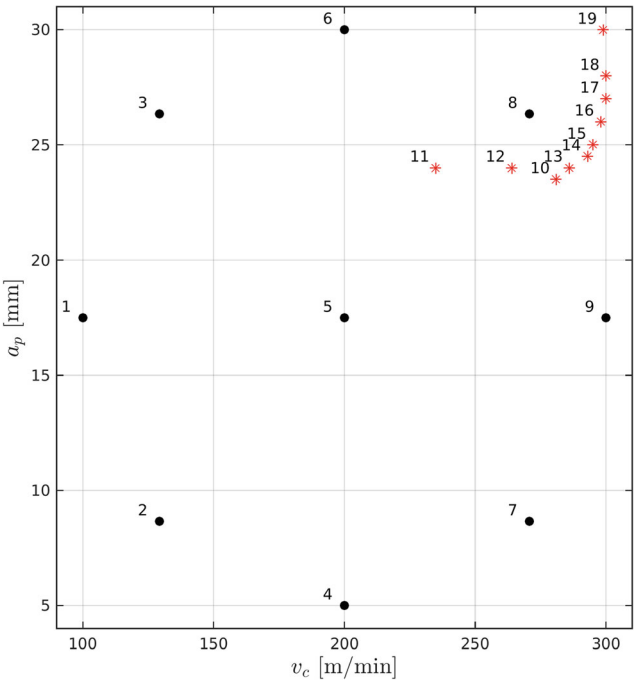

Fig. 7 Case study 1: controllable process variables values of initial experiment (dots, $\{1, 2, \ldots, 9\}$) and iteration $k = 1$ (stars, $\{10, 11, \ldots, 19\}$)

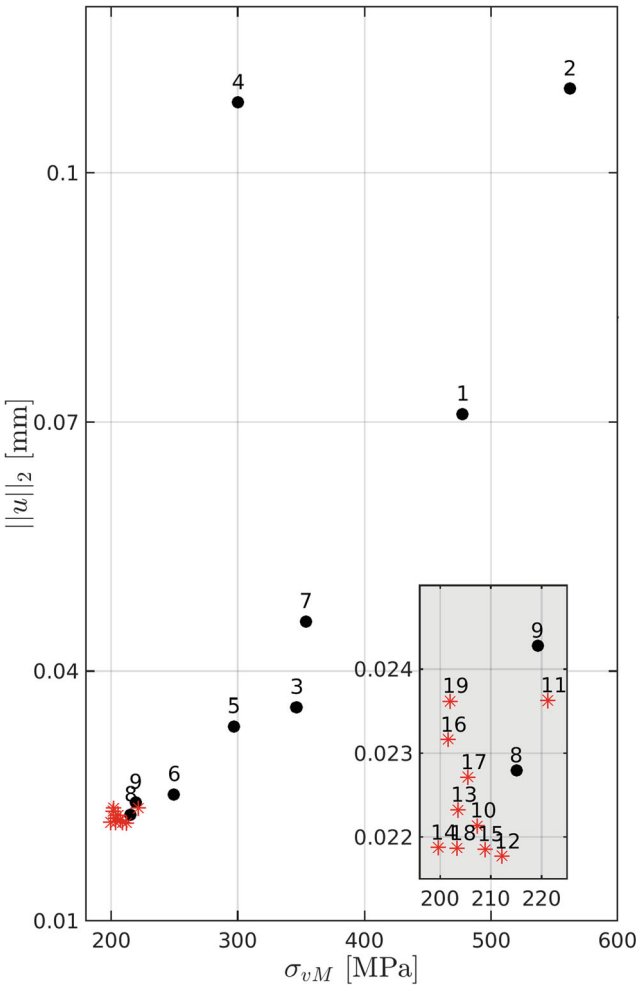

Fig. 8 Case study 1: PMs values of initial experiment (dots, $\{1, 2, \ldots, 9\}$) and iteration $k = 1$ (stars, $\{10, 11, \ldots, 19\}$). Note the zoomed area on the plot shows all of the points for the iteration $k = 1$ as well as two initial points

Matlab and ran in a PC with a 3.6 GHz Intel Core i7 processor and 16 GB 1600 MHz DDR3 of memory. Performing step 1 and 2 takes about 0.15 s, so if we compared it with the time it will take to run 10251 simulations, metamodels are an efficient way to represent simulation codes on simulation optimization algorithm.

3. *Find approximated Pareto set and front*
   Now, the Pareto front of the predicted solutions is found. The predicted Pareto front has 118 solutions. However, since the maximum number of simulations allowed per iteration $N_{\text{sim}}^{\max} = 10$, 10 solutions were selected using a max-min distance criteria algorithm with 1000 iterations. This is, 1000 subsets of 10 points were randomly selected out of the 118 points and the set which minimum distance between two points is the maximal was selected. The solutions shown as red stars on Fig. 9 are the 10 selected predicted Pareto solutions.
4. *Evaluate selected predicted Pareto solutions*
   Table 3 shows the input and output values of the 10 new runs. Figures 7 and 8 show the same results as red stars (labeled as points 10 to 19). The simulations were carried out using the same fixed parameters as the initial runs (see Table 1).
5. *Update incumbent pareto front*
   The Incumbent pareto front is updated comparing the initial incumbent Pareto front (solution 8) and the 10 new additional runs. The new Pareto solutions are 12, 14, 15, and 18.
6. *Evaluate stopping criteria*
   Next, the stopping criteria are evaluated. The criteria used here are (1) stop if the maximum number of simulations allowed was reached (no, $19 < 30$), (2) stop if R^2 of all models is larger than $1 - \varepsilon = 0.99$ (no, $R_1^2 = 0.9395$ and $R_2^2 = 0.9974$), and (3) stop if no new Pareto solutions were found (no, new solutions

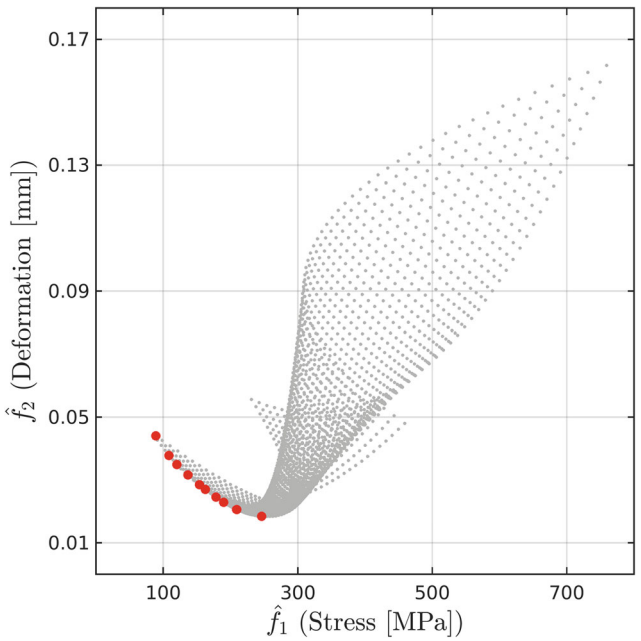

Fig. 9 Case study 1: predictions of metamodels and selected predicted Pareto aolutions (red stars)

Table 3 Case study 1: evaluation of selected predicted Pareto solutions, iteration $k = 1$

Run	v_c (m/min)	a_p (mm)	σ_{vM} (MPa)	$\|u\|_2$ (mm)
10	281.00	23.50	207.35	0.02214
11	235.00	24.00	221.27	0.02363
12	264.00	24.00	212.13	0.02177
13	286.00	24.00	203.56	0.02233
14	293.00	24.50	199.60	0.02188
15	295.00	25.00	208.83	0.02186
16	298.00	26.00	201.57	0.02316
17	300.00	27.00	205.51	0.02271
18	300.00	28.00	203.35	0.02187
19	299.00	30.00	201.92	0.02362

Table 4 Case study 1: final Pareto solutions

Run	v_c (m/min)	a_p (mm)	σ_{vM} (MPa)	$\|u\|_2$ (mm)
12	264.00	24.00	212.13	0.02177
14	293.00	24.50	199.60	0.02188
15	295.00	25.00	208.83	0.02186
18	300.00	28.00	203.35	0.02187

were found). Since none of the stopping criteria were met, a new (main) iteration is needed.

Main iteration, $k = 2$

On the second iteration, new metamodels were fitted using all available data (19 simulations). The R^2 of the new models are $R_1^2 = 0.9997$ and $R_2^2 = 0.9999$. Later, the models were used to predict a new Pareto front which only has one new solution, $\mathbf{x_{20}} = (100, 30)$. Then, a simulation run was performed at $\mathbf{x_{20}}$ and the corresponding outputs are $\mathbf{f_{20}} = (394.08, 0.04842)$. Afterwards, the incumbent Pareto front was updated but did not change. Then, the stopping criteria were evaluated and since the R^2 of both models are larger than 0.99 the method stopped and the final Pareto solutions are reported.

Report final incumbent solutions The final Pareto solutions are shown on Table 4. From this table, it can be noticed that the solutions have similar axial depth as well as deformation. However, solution 12 requires a slower cutting velocity than the other 3 solutions. In a practical application, extra information is given by the decision-maker and is in this form that we are able to select one Pareto solution and dismiss the others.

4.3 Case study 2: workpiece shape error and tool wear

To further investigate the optimization of the milling process, we now consider *workpiece shape error* (δ_x) and *tool wear* as performance measures. In this case study, the shape error and a tool wear indicator were calculated as described in the forthcoming subsections.

4.3.1 Shape error

The stress and deformation of the workpiece during the milling process, used in the first case study, are data

Table 5 Fixed process parameter values for case study 2

Variable	Value	
Radial depth of cut	$a_e = 30$	(mm)
Cutter diameter	$D = 50$	(mm)

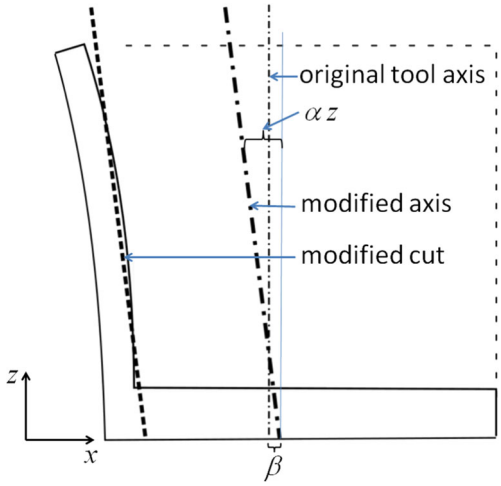

Fig. 10 Linear axis displacement and corresponding cutting edge for a bended geometry

which give information about possible incorrect material removal by the tool engagement and can be computed by the thermomechanical FEM simulation. The actual shape of the workpiece after the process is not directly given via the FEM, but by the dexel model which computes the engagement of the tool with the current workpiece geometry. Thus, an analysis of the final dexel fields and comparison with the desired dexel lengths for the correct shape can be used as a direct measure of the shape error (deformation).

In our simplified reference process, the main shape error occurs at the vertical wall, which is fixed only at the bottom and can deform freely otherwise. Thus, an examination of the dexel field with horizontal dexels in x direction, which gives the local thickness of the wall, is sufficient for detection of the main shape error.

As we can assume the existence of a tolerance for the maximal shape error to determine the validity of a workpiece, we choose the maximal deviation of dexel lengths $\|\delta_x\|$ as a measure to be minimized. Let $L(d_{\mathrm{ij}})$ denote the length of dexel d_{ij}, and $L_d(i, j)$ the corresponding desired length. Then, we define our shape error measure by

$$\|\delta_x\| := \max_{i,j} |L(d_{\mathrm{ij}}) - L_d(i, j)|. \tag{1}$$

Table 6 Process controllable variables with experimental ranges for case study 2

Variable	Value range	
Cutting velocity (v_c)	100–300	(m/min)
Axial cutting depth (a_p)	5–20	(mm)
Tool angle (α)	-2×10^{-4} - 0	(-)
Tool displacement (β)	0–0.01	(mm)

For the process considered here, the desired length for the dexel d_{ij} in the L-shaped geometry illustrated in Fig. 6 at position (y_i, z_j) is given by

$$L_d(i,j) = \begin{cases} 3 & \text{if } z_j > 5, \\ 50 & \text{if } z_j \leq 5. \end{cases}$$

4.3.2 Tool wear

In [2], Caldeirani-Filho and Diniz investigated the effect of cutting conditions on tool life, tool wear, and surface quality. Tool life (L_f) was characterized by machined length in feed direction until a flank wear of $V_{\text{Bmax}} = 0.7$ mm was reached. The corresponding units for tool life are in millimeters. They showed that tool life depends mainly on the cutting speed and presented experimental results for the processes they consider. The results (in [2], Figure 5) show an inverse linear behavior of tool life versus cutting velocity (v_c) as

$$L_f \approx \frac{7 \cdot 10^5}{v_c - 160}(\text{mm}).$$

Even without tool-life measurements available, L_f should decreases when v_c increases, as motivated in [2]. This inspired us to consider a similar formula for our process, namely

$$L_f = \frac{A}{v_c - B}, \tag{2}$$

with B chosen such that it is well below the considered range of cutting speeds.

For our process, we want to use a measure of tool-life proportional to the maximal number of workpieces which can be produced before the wear is above tolerance. Thus, the lifetime in machined length is divided by the total cut length for a single workpiece.

While the length of a single cut L_{cut} is given by the workpiece geometry, the number of cuts n_{cuts} per workpiece needed to remove all material is given via the horizontal and vertical feeds, a_e and a_p. For our reference geometry with a removed pocket of width W and height H, the number of cuts for roughing is given by $\lceil H/a_p \rceil \cdot \lceil W/a_e \rceil$ and the number of finishing cuts is $\lceil H/a_p \rceil + \lceil W/a_e \rceil - 1$.

Table 7 Case study 2: results of initial experimental design. A star in the first column indicates initial Pareto solutions

Run	v_c (m/min)	a_p (mm)	α (-)	β (mm)	$\|\delta_x\|$ (mm)	TWR (-)
1	150	8.75	-1.5×10^{-4}	2.5×10^{-3}	0.01502	0.00342
2	150	8.75	-1.5×10^{-4}	7.5×10^{-3}	0.01867	0.00342
3	150	8.75	-5.0×10^{-5}	2.5×10^{-3}	0.01419	0.00342
4	150	8.75	-5.0×10^{-5}	7.5×10^{-3}	0.01918	0.00342
5	150	16.25	-1.5×10^{-4}	2.5×10^{-3}	0.00906	0.00180
6	150	16.25	-1.5×10^{-4}	7.5×10^{-3}	0.01262	0.00180
7*	150	16.25	-5.0×10^{-5}	2.5×10^{-3}	0.00816	0.00180
8	150	16.25	-5.0×10^{-5}	7.5×10^{-3}	0.01328	0.00180
9	250	8.75	-1.5×10^{-4}	2.5×10^{-3}	0.00992	0.00722
10	250	8.75	-1.5×10^{-4}	7.5×10^{-3}	0.01864	0.00722
11	250	8.75	-5.0×10^{-5}	2.5×10^{-3}	0.00895	0.00722
12	250	8.75	-5.0×10^{-5}	7.5×10^{-3}	0.01393	0.00722
13	250	16.25	-1.5×10^{-4}	2.5×10^{-3}	0.00787	0.00380
14	250	16.25	-1.5×10^{-4}	7.5×10^{-3}	0.00673	0.00380
15*	250	16.25	-5.0×10^{-5}	2.5×10^{-3}	0.00527	0.00380
16	250	16.25	-5.0×10^{-5}	7.5×10^{-3}	0.01027	0.00380
17*	100	12.50	-1.0×10^{-4}	5.0×10^{-3}	0.01681	0.00104
18	300	12.50	-1.0×10^{-4}	5.0×10^{-3}	0.00807	0.00624
19	200	5.00	-1.0×10^{-4}	5.0×10^{-3}	0.01742	0.00784
20	200	20.00	-1.0×10^{-4}	5.0×10^{-3}	0.00846	0.00280
21	200	12.50	-2.0×10^{-4}	5.0×10^{-3}	0.00934	0.00364
22	200	12.50	0.0×10^{0}	5.0×10^{-3}	0.01081	0.00364
23	200	12.50	-1.0×10^{-4}	0.0×10^{0}	0.00911	0.00364
24	200	12.50	-1.0×10^{-4}	10×10^{-3}	0.01480	0.00364
25	200	12.50	-1.0×10^{-4}	5.0×10^{-3}	0.00980	0.00364

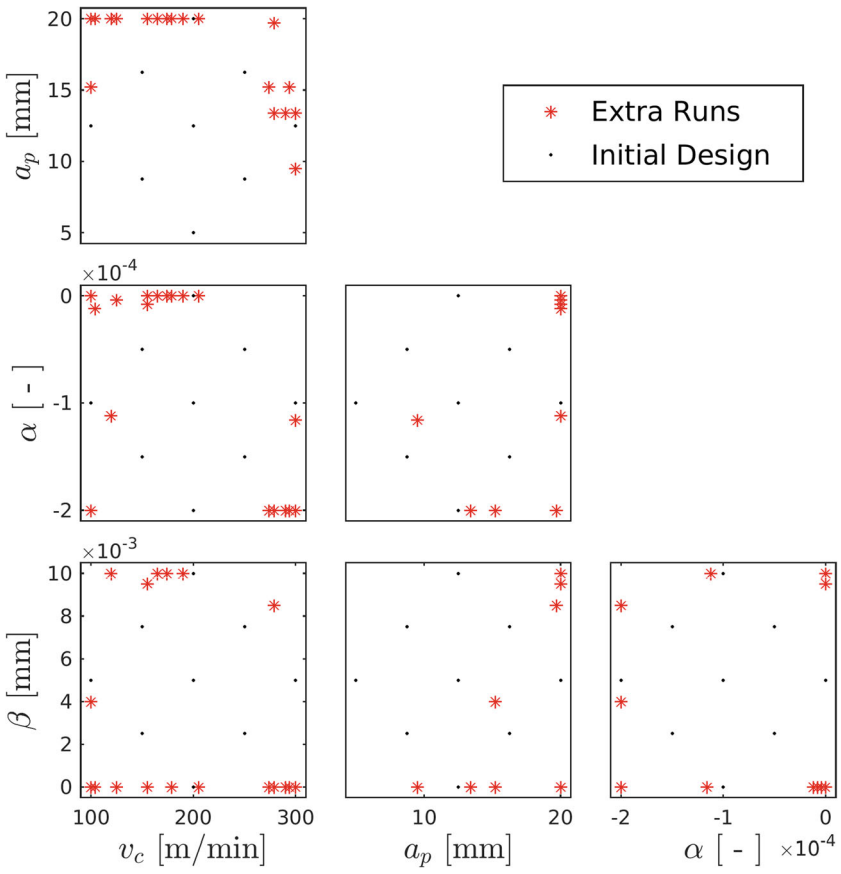

Fig. 11 Case study 2: 2D projections of evaluated controllable process variables. Initial design (black dots) and extra runs (red stars)

Thus, we choose a dimensionless measure for tool wear rate per workpiece (TWR) as the inverse of the number of producible workpieces,

$$\mathrm{TWR} = \frac{n_{\mathrm{cuts}} L_{\mathrm{cut}}}{L_f} = \frac{v_c - B}{\tilde{A}} \left(\left\lceil \frac{H}{a_p} \right\rceil \cdot \left(\left\lceil \frac{W}{a_e} \right\rceil + 1 \right) + \left\lceil \frac{W}{a_e} \right\rceil - 1 \right). \tag{3}$$

For the process considered here, we have

$H = 45$ (mm), $W = 47$ (mm)

and choose

$\tilde{A} = 5 \cdot 10^5$ (m/min), $B = 60$ (m/min).

4.3.3 Process controllable variables

Four process controllable variables were considered in this case: cutting velocity (v_c), axial cutting depth (a_p), tool angle (α), and tool displacement (β). Fixed parameters which differ from case study 1 are listed in Table 5, and the rest are as in Table 1.

The thermomechanical deformation during the process can be compensated by a variation of the tool path. For a three dimensional workpiece, there are typically quite complex tool paths and corresponding possibilities for path variations. For our simplified reference workpiece, a simple class of tool path variations is given by a linear displacement ad(z) of the axis in x direction, which is used (only) for the

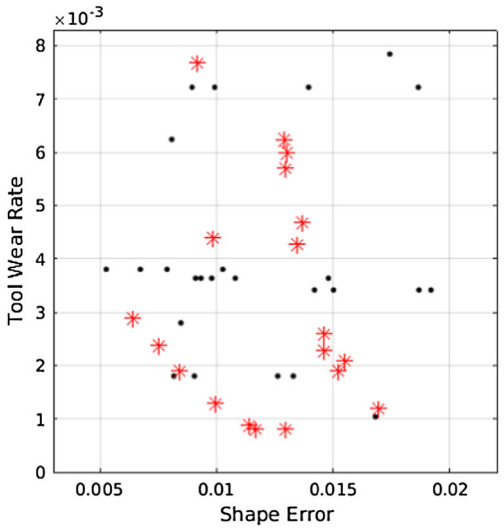

Fig. 12 Case study 2: performance measure values of evaluated runs. Initial design (black dots) and extra runs (red stars)

Table 8 Case study 2: evaluation of selected predicted Pareto solutions. Iterations are divided by horizontal lines. Iteration 1: solution 26, Iteration 2: 27 to 32, iteration 3: 33 to 38, iteration 4: 39 to 44

Run	v_c (m/min)	a_p (mm)	α (-)	β (mm)	$\|\delta_x\|$ (mm)	TWR [-]
26	100	20.00	0.00×10^{0}	0.0×10^{0}	0.01167	0.00080
27	104	20.00	-1.20×10^{-5}	0.0×10^{0}	0.01139	0.00088
28	155	20.00	-8.00×10^{-6}	0.0×10^{0}	0.00838	0.00190
29	125	20.00	-4.00×10^{-6}	0.0×10^{0}	0.00995	0.00130
30	179	20.00	0.00×10^{0}	0.0×10^{0}	0.00753	0.00238
31	205	20.00	0.00×10^{0}	0.0×10^{0}	0.00642	0.00290
32	279	19.70	-2.00×10^{-4}	8.5×10^{-3}	0.00983	0.00438
33	300	9.50	-1.16×10^{-4}	0.0×10^{0}	0.00915	0.00768
34	100	15.20	-2.00×10^{-4}	4.0×10^{-3}	0.01294	0.00080
35	155	20.00	0.00×10^{0}	9.5×10^{-3}	0.01521	0.00190
36	165	20.00	0.00×10^{0}	10×10^{-3}	0.01549	0.00210
37	174	20.00	0.00×10^{0}	10×10^{-3}	0.01461	0.00228
38	190	20.00	0.00×10^{0}	10×10^{-3}	0.01462	0.00260
39	279	13.40	-2.00×10^{-4}	0.0×10^{0}	0.01296	0.00569
40	290	13.40	-2.00×10^{-4}	0.0×10^{0}	0.01303	0.00598
41	300	13.40	-2.00×10^{-4}	0.0×10^{0}	0.01289	0.00624
42	274	15.20	-2.00×10^{-4}	0.0×10^{0}	0.01343	0.00428
43	294	15.20	-2.00×10^{-4}	0.0×10^{0}	0.01367	0.00468
44	120	20.00	-1.12×10^{-4}	10×10^{-3}	0.01693	0.00120

finishing cuts at the vertical wall. We consider here the same variation for the whole finishing process at the wall,

$$\mathrm{ad}(z) = \alpha z + \beta,$$

which moves the originally vertical tool axis at x_* to a shifted and inclined axis at $x_* + \mathrm{ad}(z)$. This results in a corresponding displacement of the cutting edge, see Fig. 10. This gives two scalar control variables, α (in first approximation, for small values, this is the tool-axis inclination angle) and β (the horizontal tool displacement).

Connecting both variables α and β, the slope of the applied cutting tool is modified. Considering negative values for α mean that the tool will consider the outward tilting of the vertical wall and will compensate this. Additionally, the tool might also be shifted towards or outwards from the L-shaped geometry.

The process controllable variables and the experimental ranges considered are given in Table 6. The rest of the process variables are considered as fixed and the values differing from Table 1 are listed in Table 5.

4.3.4 Optimization results

As in case study 1, the optimization was conducted following the flow chart in Fig. 5. The optimization parameters used here are: maximum number of simulations $N_{\mathrm{sim}}^{\mathrm{total}} = 60$; maximum number of simulations per iteration $N_{\mathrm{sim}}^{max} = 6$; and the lower bound for R^2 was set at 99% ($\varepsilon = 0.01$).

The initial design of experiments is a central composite design with 25 runs. Table 7 shows the values of the CVs and the corresponding PMs evaluations. The CVs and PMs values are also shown graphically on Figs. 11 and 12 as black dots. The initial Pareto solutions are solutions 7, 15, and 17.

Table 9 Case study 2: final Pareto solutions

Simulation	v_c (m/min)	a_p (mm)	α (-)	β (mm)	$\|\delta_x\|$ (mm)	TWR (-)
15	250	16.25	-5.0×10^{-5}	2.5×10^{-3}	0.00527	0.00380
31	205	20.00	0.0×10^{0}	0.0×10^{0}	0.00642	0.00290
30	179	20.00	0.0×10^{0}	0.0×10^{0}	0.00753	0.00238
7	150	16.25	-5.0×10^{-5}	2.5×10^{-3}	0.00816	0.00180
29	125	20.00	-4.0×10^{-6}	0.0×10^{0}	0.00995	0.00130
27	104	20.00	-1.2×10^{-5}	0.0×10^{0}	0.01139	0.00088
26	100	20.00	0.0×10^{0}	0.0×10^{0}	0.01167	0.00080

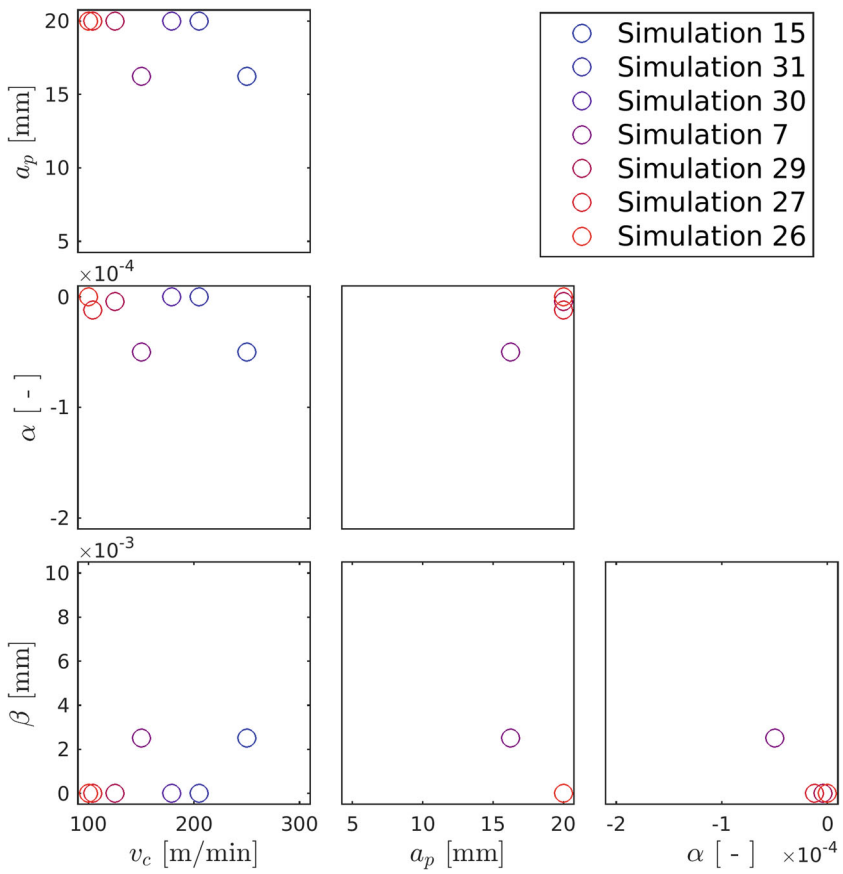

Fig. 13 Case study 2: 2D projections of final Pareto set

After the initial data is collected, a MLR model was fitted to estimate workpiece shape error and tool wear rate was calculated using Eq. 3.

The R^2 of the metamodel for shape error is 0.9852. Then, the performance measures values of 10,978,821 ($201 \times 51 \times 51 \times 21$) solutions were estimated and the predicted Pareto Front identified. The predicted Pareto front at iteration $k = 1$ has 1 solution $\mathbf{x_{26}} = (100, 30, 0, 0)$. Then, a simulation run was performed and the corresponding outputs are $\mathbf{f_{26}} = (0.01167, 0.00080)$. The incumbent Pareto front is then updated and the new Pareto solutions are 7, 15, and 26. Since, none of the stopping criteria are met a new iteration began.

A total of 4 iterations and 44 simulation runs were performed until the method stopped. Table 8 shows the results of the 19 additional runs. Solution 26 is for iteration 1, 27 to 32 for iteration 2, 33 to 38 from iteration 3 and 39 to 44 for iteration 4. The methods stopped because the R^2 of the metamodels were grater that the lower limit.

The final Pareto solutions are reported on Table 9. They correspond to simulation run 7, 15, 26, 27, 29, 30, and 31. The final Pareto set and front are shown graphically on Figs. 13 and 14.

4.3.5 Optimization results interpretation

From the data in the Pareto set (Fig. 13), 4 clusters of solutions can be observed:

- Cluster 1: simulations 26, 27, and 29, corresponds to low values of tool wear rate, in which case it is necessary to set the process at a low cutting velocity, high axial depth, large tool angle, and none tool displacement.
- Cluster 2: simulation 15, corresponds to a workpiece with low shape error. In this case, it is recommended to use a hight cutting velocity, low axial depth, large tool angel, and low tool displacement.
- Cluster 3: simulation 7, consisting of a compromise between both optimization goals, tending to sightly prefer small shape error over low tool wear rate.
- Cluster 4: simulations 30 and 31, being also a compromise but tending to give similar importance to both optimization goals.

As mentioned before, the information described in the clusters is intended to serve as guide for manufacturing engineers in charge of setting the process parameters, and

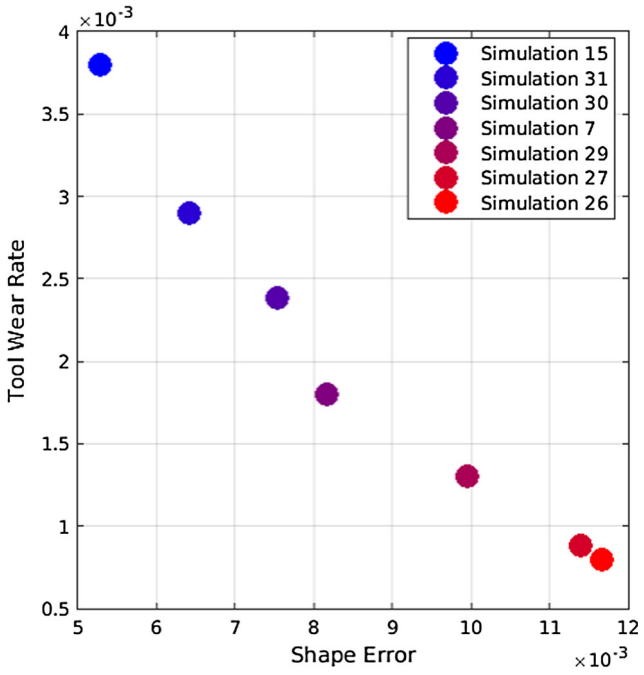

Fig. 14 Case study 2: final Pareto front

depending on the relevance of each performance measure at a particular time in the production process they can select a specific solution.

5 Conclusion

In summary, we presented the thermomechanic problem on a milling process and used a sequential surrogate based multiobjective simulation optimization method to solve two case studies of a machining process on 1.1191 steel. The goal was to find the controllable process variables that optimize two performance measures simultaneously. In general, the method was able to approximate a Pareto front in a modest number of evaluations, which is critical for the cases of interest where a single simulation or experimental run can be costly and time-consuming.

Especially, for the second case study, we managed to solve a fourth dimensional variable space with only 44 computational simulations and were able to find several clusters of Pareto-optimal solutions from which a decision-maker can pick the most suitable solution for the specific needs at any production time.

The optimization of process parameters on the reduced L-shaped workpiece geometry is meant and presented as a case study for the applicability and potential use of simulation-based optimization methods. For scenarios where the results could be verified by a comparison with experiments, more complex geometries (with more precise boundary conditions) would have to be considered, which typically need much larger computing resources for each simulation. The accuracy of the simulation method was already verified for the (still quite simple) workpiece presented in Section 2.2, results of the simulation compare very well with experimental data for sets of process parameters considered in [5].

As future work, we aim to apply the optimization method to thermomechanical case studies with more than 2 PMs. Also, we will investigate how to asses process variability either by using simulation models and/or physical experimentation and we will introduce a multiobjective optimization method based on stochastic surrogate models. In addition, possible improvements of the simulated model like models considering non-linear elasticity or plastic effects using temperature dependent material properties will be explored. Furthermore, more complex sets of parameters will be consider in the optimize. For example, tool axis displacements could be considered not only in one position but along the whole tool path.

Acknowledgments The authors gratefully acknowledge the financial support by the Mexican National Council for Science and Technology (CONACYT) and the German Academic Exchange Service (DAAD) through the project "Simulación Numérica y Optimización para Procesos Dependientes del Tiempo en Ingeniería y Ciencias de los Materiales" ("Numerical Simulation and Optimization of Time Dependent Processes in Engineering and Materials Science"). The support given by the German Research Foundation (DFG) to the project "Thermomechanical Deformation of Complex Workpieces in Drilling and Milling Processes" within the DFG Priority Program 1480 "Modeling, Simulation and Compensation of Thermal Effects for Complex Machining Processes" is also acknowledged.

References

1. Barton RR (2009) Simulation optimization using metamodels. In: Winter Simulation Conference, pp 230–238. Winter Simulation Conference
2. Caldeirani-Filho J, Diniz AE (2002) Influence of cutting conditions on tool life, tool wear and surface finish in the face milling process. J Braz Soc Mech Sci 24(1):10–14. https://doi.org/10.1590/S0100-73862002000100002
3. Denkena B, Maaß P, Schmidt A, Niederwestberg D, Vehmeyer J, Niebuhr C, Gralla P (2017) Thermomechanical deformation of complex workpieces in milling and drilling processes. In: Biermann D, Hollmann F (eds) Thermal Effects in Complex Machining Processes - Final Report of the DFG Priority Program 1480, LNPE Series. Springer. to appear, p 32
4. Denkena B, Schmidt A, Henjes J, Niederwestberg D, Niebuhr C (2013) Modeling a thermomechanical NC-simulation. Procedia CIRP 8:69–74
5. Denkena B, Schmidt A, Maaß P, Niederwestberg D, Niebuhr C, Vehmeyer J (2015) Prediction of temperature induced shape deviations in dry milling. Procedia CIRP 31:340–345
6. Dong S, Chunsheng E, Fan B, Danai K, Kazmer DO (2007) Process-driven input profiling for plastics processing. J Manuf Sci Eng 129(4):802–809
7. Jin R, Chen W, Sudjianto A (2002) On sequential sampling for global metamodeling in engineering design. In: ASME 2002

International Design Engineering Technical Conferences and Computers and Information in Engineering Conference, pp 539–548. American Society of Mechanical Engineers
8. Kok SW, Tapabrata R (2005) A framework for design optimization using surrogates. Eng Optim 37(7):685–703. https://doi.org/10.1080/03052150500211911
9. Li J, Yang X, Ren C, Chen G, Wang Y (2015) Multiobjective optimization of cutting parameters in ti-6al-4v milling process using nondominated sorting genetic algorithm-ii. Int J Adv Manuf Technol 76(5):941–953. https://doi.org/10.1007/s00170-014-6311-8
10. Li YF, Ng SH, Xie M, Goh TN (2010) A systematic comparison of metamodeling techniques for simulation optimization in decision support systems. Appl Soft Comput 10(4):1257–1273. https://doi.org/10.1016/j.asoc.2009.11.034
11. Montalvo-Urquizo J, Akbay Z, Schmidt A (2009) Adaptive finite element models applied to the laser welding problem. Comput Mater Sci 46(1):245–254. https://doi.org/10.1016/j.commatsci.2009.02.037
12. Montalvo-Urquizo J, Bobrov P, Schmidt A, Wosniok W (2012) Elastic responses of texturized microscale materials using FEM simulations and stochastic material properties. Mechanics of Materials 47:1–10. https://doi.org/10.1016/j.mechmat.2011.11.008
13. Niebuhr C, Niederwestberg D, Schmidt A (2014) Finite element simulation of macroscopic machining processes – implementation of time dependent domain and boundary conditions. Berichte aus der Technomathematik, Universität Bremen, pp 14–01
14. Qu S, Zhao J, Wang T (2017) Experimental study and machining parameter optimization in milling thin-walled plates based on nsga-ii. Int J Adv Manuf Technol 89(5):2399–2409. https://doi.org/10.1007/s00170-016-9265-1
15. Rao RV (2011) Advanced modeling and optimization of manufacturing processes. Springer Series in Advanced Manufacturing, Berlin
16. Schmidt A, Bänsch E, Jahn M, Luttmann A, Niebuhr C, Vehmeyer J (2017) Optimization of engineering processes icluding heating and time-dependent domains. In: Bociu L, Desideri J, Habbal A (eds) System Modeling and Optimization, 27th IFIP TC 7 Conference, CSMO 2015, IFIP AICT Series, vol 494, pp 452–461. Springer
17. Schmidt A, Siebert K (2005) Design of adaptive finite element software: the finite element toolbox ALBERTA. Springer Heidelberg, Berlin
18. Simpson TW, Poplinski JD, Koch PN, Allen JK (2001) Metamodels for computer-based engineering design: survey and recommendations. Engineer Comput 17(2):129–150
19. Smith GT (2008) Cutting tool technology: industrial handbook. Springer, London. https://doi.org/10.1007/978-1-84800-205-0
20. Suhr B (2010) Simulation of steel quenching with interaction of classical plasticity and TRIP: numerical methods and model comparison. Logos Verlag, Berlin
21. Tschätsch H, Reichelt A (2009) Milling. In: Applied Machining Technology, pp 173–223. Springer Berlin Heidelberg, Berlin, Heidelberg. https://doi.org/10.1007/978-3-642-01007-1
22. Villarreal-Marroquin MG, Cabrera-Rios M, Castro JM (2011) A multicriteria simulation optimization method for injection molding. J Polym Eng 31(5):397–407
23. Villarreal-Marroquin MG, Po-Hsu C, Mulyana R, Santner TJ, Dean AM, Castro JM (2016) Multiobjective optimization of injection molding using a calibrated predictor based on physical and simulated data. Polymer Engineering & Science
24. Villarreal-Marroqun MG, Svenson JD, Sun F, Santner TJ, Dean AM, Castro JM (2013) A comparison of two metamodel-based methodologies for multiple criteria simulation optimization using an injection molding case study. J Polym Eng 33(3):193–209
25. Wang GG, Shan S (2007) Review of metamodeling techniques in support of engineering design optimization. J Mech Des 129(4):370–380
26. Zhou H (2012) Computer modeling for injection molding: simulation, optimization, and control. Wiley, New York